

The de Haas-van Alphen quantum oscillations in the kagome metal $RbTi_3Bi_5$

Zixian Dong(董自仙), Lei Shi(石磊), Bin Wang(王彬), Mengwu Huo(霍梦五), Xing Huang(黄星), Chaoxin Huang(黄潮欣), Peiyue Ma(马培跃), Yunwei Zhang(张云蔚), Bing Shen(沈冰), and Meng Wang(王猛)

Citation: Chin. Phys. B, 2024, 33 (**10**): 107102. DOI: 10.1088/1674-1056/ad6a0a
Journal homepage: http://cpb.iphy.ac.cn; http://iopscience.iop.org/cpb

What follows is a list of articles you may be interested in

Two-dimensional Sb net generated nontrivial topological states in $SmAgSb_2$ probed by quantum oscillations

Jian Yuan(袁健), Xian-Biao Shi(石贤彪), Hong Du(杜红), Tian Li(李田), Chuan-Ying Xi(郗传英), Xia Wang(王霞), Wei Xia(夏威), Bao-Tian Wang(王保田), Rui-Dan Zhong(钟瑞丹), and Yan-Feng Guo(郭艳峰)
Chin. Phys. B, 2024, 33 (**7**): 077102. DOI: 10.1088/1674-1056/ad4bc2

Recent progress on excitation and manipulation of spin-waves in spin Hall nano-oscillators

Liyuan Li(李丽媛), Lina Chen(陈丽娜), Ronghua Liu(刘荣华), and Youwei Du(都有为)
Chin. Phys. B, 2020, 29 (**11**): 117102. DOI: 10.1088/1674-1056/abaed5

In-situ SiN combined with etch-stop barrier structure for high-frequency AlGaN/GaN HEMT

Min-Han Mi(宓珉瀚), Sheng Wu(武盛), Ling Yang(杨凌), Yun-Long He(何云龙), Bin Hou(侯斌), Meng Zhang(张濛), Li-Xin Guo(郭立新), Xiao-Hua Ma(马晓华), Yue Hao(郝跃)
Chin. Phys. B, 2020, 29 (**4**): 047104. DOI: 10.1088/1674-1056/ab7746

Negative differential resistance and quantum oscillations in $FeSb_2$ with embedded antimony

Fangdong Tang(汤方栋), Qianheng Du(杜乾衡), Cedomir Petrovic, Wei Zhang(张威), Mingquan He(何明全), Liyuan Zhang(张立源)
Chin. Phys. B, 2019, 28 (**3**): 037104. DOI: 10.1088/1674-1056/28/3/037104

Quantum oscillation measurements in high magnetic field and ultra-low temperature

Pu Wang(王瀑), Gang Li(李岗), Jian-Lin Luo(雒建林)
Chin. Phys. B, 2018, 27 (**7**): 077101. DOI: 10.1088/1674-1056/27/7/077101

The de Haas–van Alphen quantum oscillations in the kagome metal $RbTi_3Bi_5$

Zixian Dong(董自仙), Lei Shi(石磊), Bin Wang(王彬), Mengwu Huo(霍梦五), Xing Huang(黄星), Chaoxin Huang(黄潮欣), Peiyue Ma(马培跃), Yunwei Zhang(张云蔚)[†], Bing Shen(沈冰)[‡], and Meng Wang(王猛)[§]

Center for Neutron Science and Technology, Guangdong Provincial Key Laboratory of Magnetoelectric Physics and Devices, School of Physics, Sun Yat-Sen University, Guangzhou 510275, *China*

(Received 21 May 2024; revised manuscript received 18 July 2024; accepted manuscript online 1 August 2024)

The kagome system has attracted great interest in condensed matter physics due to its unique structure that can host various exotic states such as superconductivity (SC), charge density waves (CDWs) and nontrivial topological states. The topological semimetal $RbTi_3Bi_5$ consisting of a Ti kagome layer shares a similar crystal structure to the topological correlated materials AV_3Sb_5 (A = K, Rb, Cs) but without the absence of CDW and SC. Systematic de Haas–van Alphen oscillation measurements are performed on single crystals of $RbTi_3Bi_5$ to pursue nontrivial topological physics and exotic states. Combining this with theoretical calculations, the detailed Fermi surface topology and band structure are investigated. A two-dimensional Fermi pocket β is revealed with a light effective mass, consistent with the semimetal predictions. The Landau fan diagram of $RbTi_3Bi_5$ reveals a zero Berry phase for the β oscillation in contrast to that of $CsTi_3Bi_5$. These results suggest that kagome $RbTi_3Bi_5$ is a good candidate for exploring nontrivial topological exotic states and topological correlated physics.

Keywords: oscillation, Fermi surface, band structure

PACS: 71.18.+y, 52.70.Ds, 71.20.–b **DOI:** 10.1088/1674-1056/ad6a0a

1. Introduction

The kagome lattice with corner-sharing triangles has relativistic band crossings at the Brillouin zone (BZ) corners and usually hosts various exotic states.[1–4] Two-dimensional kagome superconductors AV_3Sb_5 (A = K, Rb, Cs) were recently discovered and have attracted significant interest in condensed matter physics. Theoretical and experiment investigations reveal a Z_2 nontrivial topological band structure with multiple protected Dirac crossings and van Hove singularities (vHSs).[5,6] Around 80–100 K, the system undergoes a chiral charge density wave transition with an orbital moment.[7–12] Accompanying this transition, the prominent anomalous and planar Hall effects exhibit unconventional behaviors.[13–15]. Besides this first-order transition, nuclear magnetic resonance and muon spin relaxation measurements reveal other transitions below the charge density wave (CDW) transition with a sharp increase in electronic chiral anisotropy.[16–19]

To pursue the origin of these exotic orders and the interplay of the correlation effect and nontrivial topology, various experiments have been performed, revealing a complicated electronic phase diagram.[20,21] The chiral CDW and superconductivity (SC) orders are sensitive to pressure and chemical doping.[22–25] The observed multiple modulations suggest the emergence of various CDW phases and electronic nematic states. Two domes of SC were observed in the phase diagram and considered to originate from different mechanisms.[26–28] The interplay of SC and CDWs is still puzzling and challenging. The analog ATi_3Bi_5 (A = Rb, Cs) share a similar crystal structure to AV_3Sb_5 (A = K, Rb, Cs) with a kagome layer made of Ti.[29,30] Theoretical calculations and experimental results yielded a similar nontrivial topological band structure.[31–34] However, the experimental studies suggested the absence of the chiral CDW in ATi_3Bi_5 (A = Rb, Cs) and revealed different electron phase diagrams from AV_3Sb_5 (A = K, Rb, Cs).[35] Thus ATi_3Bi_5 (A = Rb, Cs) can provide a new means to explore the mechanism of electronic nematicity and its interplay with the orbital degree of freedom in these kagome compounds.[32,36] Detailed investigations of band structure and Fermi topology are desirable for a better understanding of the interplay between electron magnetism and the lattice in topologically correlated systems.

In this work, we perform systematic magnetization measurements on single crystals of $RbTi_3Bi_5$. Above 7 T, prominent de Haas–van Alphen (dHvA) oscillations are observed and a light effective mass is revealed. In contrast to $CsTi_3Bi_5$,[37] only one frequency of oscillation is identified. Combined with theoretical calculations and angular dHvA oscillation measurements, the two-dimensional (2D) Fermi surface topology is characterized. The Landau fan diagram reveals a zero Berry phase for this oscillation. This is consistent with the theoretical prediction of a Z_2 nontrivial topological

[†]Corresponding author. E-mail: zhangyunw@mail.sysu.edu.cn
[‡]Corresponding author. E-mail: shenbing@mail.sysu.edu.cn
[§]Corresponding author. E-mail: wangmeng5@mail.sysu.ed.cn

© 2024 Chinese Physical Society and IOP Publishing Ltd

phase. The absence of CDW suggests different correlation effects in this topological kagome system.

2. Experiments

Single crystals of $RbTi_3Bi_5$ were synthesized using the self-flux method.[38] In an argon glovebox, Rb (liquid, Alfa 99.98%), Ti (powder, Alfa 99.99%) and Bi (powder, Alfa 99.99%) with a molar ratio of Rb:Ti:Bi = 1:2:6 were put into a crucible. The crucible was then sealed in a vacuumed quartz tube. The mixture was first heated to 1000 °C for 48 h and cooled down to 600 °C at 20 min·°C^{-1}. The crystals were separated from the flux by centrifuging the mixture. The crystal structure was investigated by x-ray diffraction. Electrical transport measurements were carried out in a physical property measurement system (Quantum Design). The magnetization measurements were performed with a vibrating sample magnetometer. Density functional theory (DFT) calculations were performed using the Vienna *ab initio* package.[39,40] The Perdew–Burke–Ernzerhof type generalized approximation was used to describe the exchange–correlation function.[41] Lattice relaxations were performed until the force was less than 0.001 eV·Å^{-1}. The plane-wave cutoff energy was 600 eV and the k mesh was $20 \times 20 \times 12$ in the optimization and self-consistent calculations. The Fermi surfaces were generated using a dense k-mesh grid of $20 \times 20 \times 20$ and visualized using the XCRYSDEN software package.[42] The quantum oscillation frequencies were calculated using the SKEAF code.[43]

3. Results and discussion

$RbTi_3Bi_5$ exhibits a layered crystal structure consisting of Ti–Bi slabs intercalated by Rb cations, as shown in Figs. 1(a) and 1(b). The Ti sublattice forms a perfect 2D kagome net. Our measurements are based on planar single crystals. The (00l) diffraction peaks are revealed by the x-ray diffraction measurements. The temperature-dependent resistivity $\rho(T)$, shown in Fig. 1(c), exhibits a metallic behavior with the absence of the anomaly for CDW transition.

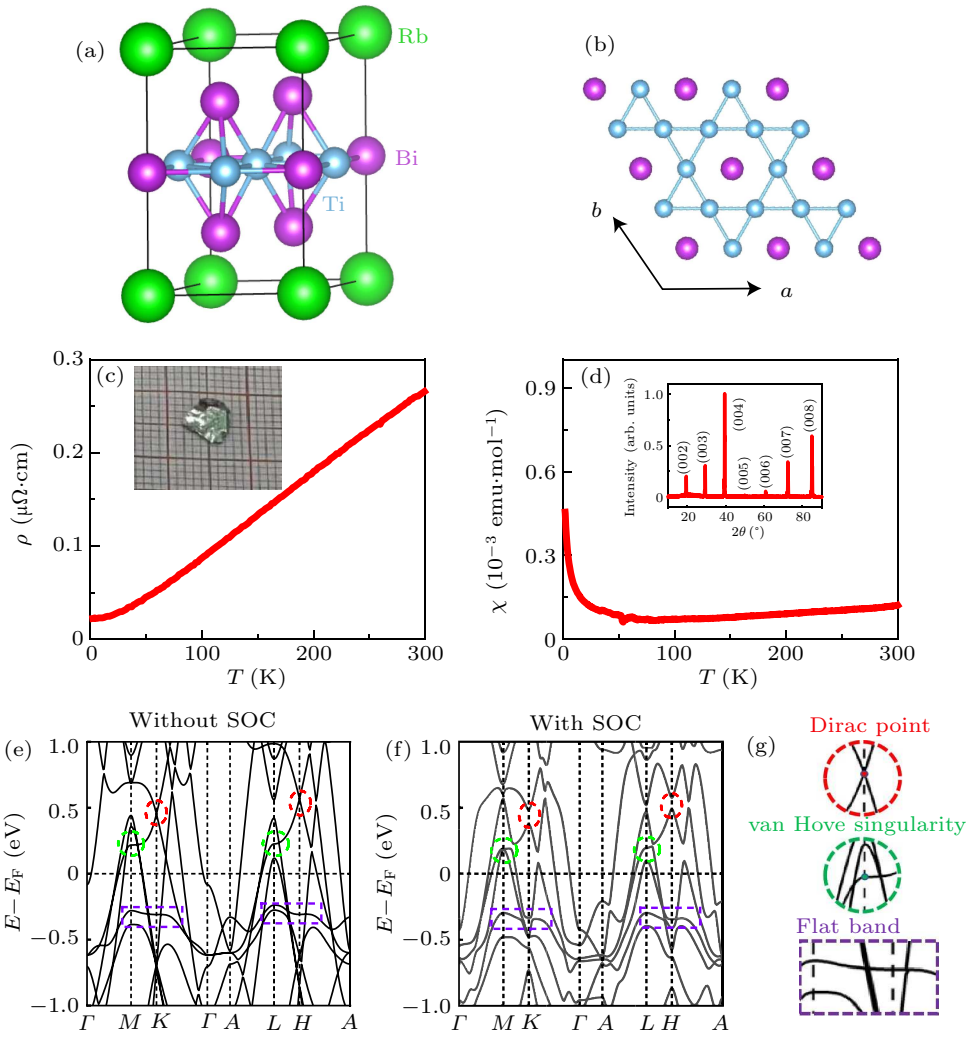


Fig. 1. (a) The crystal structure of $RbTi_3Bi_5$. (b) A two-dimensional kagome plane consisting of Bi and Ti. (c) Temperature dependence of the resistivity. The inset is a photo of a typical single crystal. (d) Temperature dependence of magnetic susceptibility with $\mu_0 H = 1$ T along the c-axis during zero field cooling. The inset shows the x-ray diffraction pattern of a single crystal of $RbTi_3Bi_5$. (e), (f) Band structures of $RbTi_3Bi_5$ without spin–orbit coupling (SOC) (e) and with SOC (f). (g) The band structure of the Dirac point, van Hove singularity and flat bands are marked by red, green and purple dashed lines, respectively.

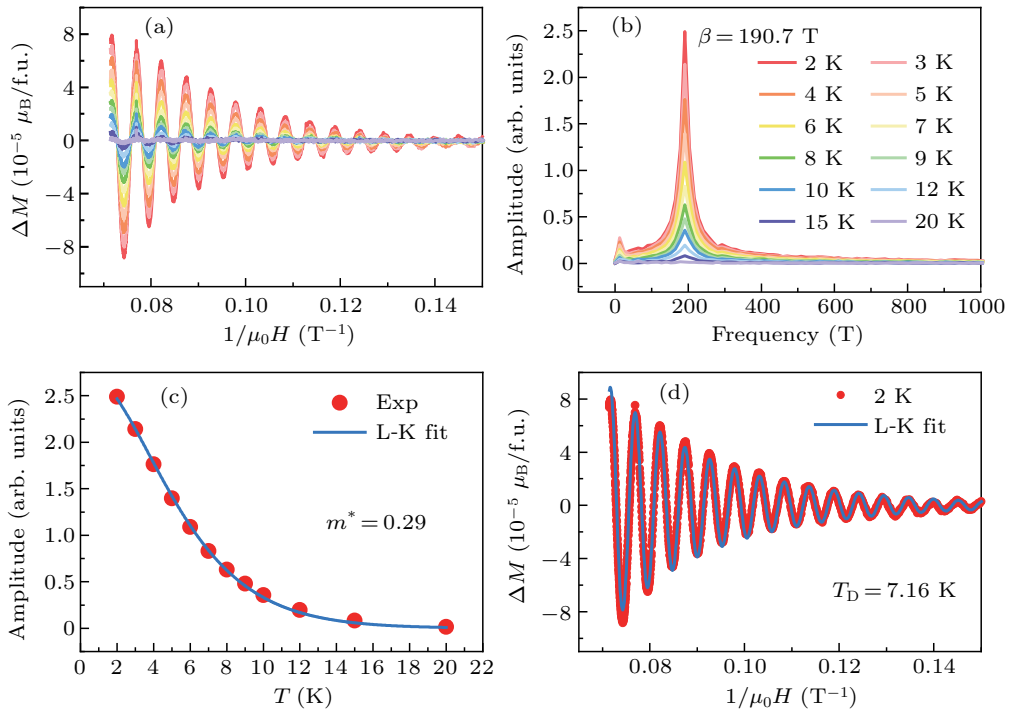


Fig. 2. (a) Magnetization after subtraction of a monotonic background ΔM as a function of $1/(\mu_0 H)$ at various temperatures with a magnetic field along the c-axis. (b) FFT spectra of ΔM. The oscillation frequency is denoted as β. (c) Temperature dependence of the FFT amplitudes of the oscillations in (b). The solid curve represents the best fit to the data using the L-K formula, where the effective mass m^* can be obtained. (d) The oscillation of the subtracted magnetization at 2 K. The red line is the experimental data and the blue line is the L-K fit. The Dingle temperature T_D is 7.1 K.

Correspondingly, the temperature-dependent susceptibility $\chi(T)$ (defined as M/H) exhibits a paramagnetic behavior, and no phase-transition anomaly is observed over the whole temperature region in Fig. 1(d). These results suggest that the absence of CDW in $RbTi_3Bi_5$ is consistent with a former report.[44] Besides, no SC is observed in $\rho(T)$ and $\chi(T)$ upon decreasing the temperature to 2 K. The absence of CDW and SC compared with AV_3Sb_5 motivated us to investigate the electronic structure of $RbTi_3Bi_5$. The DFT calculations reveal several nontrivial topological band structures in Figs. 1(e) and 1(f). The flat electronic band as a typical characteristic of the kagome lattice emerges around a binding energy of 0.3 eV. At the K point, a type-II nodal line is observed. The vHS emerges around the M point and is close to the Fermi level (E_F). These exotic electronic features are very similar to those in AV_3Sb_5 compounds. The obvious difference between AV_3Sb_5 and $RbTi_3Bi_5$ motivated us to further check these theoretical results by experiment to pursue the different correlation effects in the kagome topological system.

Compared with the Shubnikov–de Haas (electronic transport) quantum oscillation measurements, the dHvA (magnetic) quantum oscillation measurements are insensitive to extrinsic surface states and conditions and provide Fermi topology information from the bulk. In our experiments, a planar single crystal of $RbTi_3Bi_5$ was mounted in a wedge-shaped quartz holder with various thicknesses to control the sample plane direction. The isothermal magnetization of $RbTi_3Bi_5$ was measured with an applied field (B) parallel to the c-axis. At 2 K, quantum oscillations were observed above 7 T. After subtracting the polynomial background, remarkable periodic oscillations in $\Delta M(H)$ versus $1/(\mu_0 H)$ curves are more obvious, as shown in Fig. 2(a). With increasing temperature these oscillations gradually become invisible and eventually disappear around 20 K. To analyze these oscillations, a fast Fourier transform (FFT) is performed, and the related spectra are depicted in Fig. 2(b). An obvious peak is identified at 190 T, consistent with previous Shubnikov–de Haas quantum oscillation results. A weak peak was also identified around a smaller frequency of 12 T after careful checking by subtracting various polynomial backgrounds. According to the Lifshitz–Kossevich (L-K) formula, the oscillatory ΔM can be expressed as[45,46]

$$\Delta M \propto \sqrt{B} R_T R_D R_S \sin\left[2\pi\left(\frac{F}{B} - \frac{1}{2} + \frac{\phi_B}{2\pi} - \delta\right)\right],$$

where

$$R_T = (\alpha m^* T/(\mu_0 B))/\sinh(\alpha m^* T/(\mu_0 B)),$$

$R_D = \exp(-\alpha m^* T_D/(\mu_0 B))$ and $R_S = \cos(\pi m^* g^*)$. The parameter α is a constant defined as $\alpha = 14.69$ T/K, m^* is the cyclotron effective mass, T_D is the Dingle temperature, g^* is the effective g factor, δ is the phase shift and δ is 0 for a 2D system and $\pm 1/8$ for a three-dimensional system. The effective mass m^* for an oscillation of 190 T is calculated to be $0.29 m_e$. The light effective mass indicates a typical semimetallic band dispersion in agreement with our calculations below and close to that in $CsTi_3Bi_5$.[47] The Dingle temperature T_D at 2 K is calculated to be 7.164 K, and the corresponding mean free path is 514.024 nm. More detailed results are summarized in Table 1.

Table 1. Parameters derived from dHvA oscillations for $RbTi_3Bi_5$. The frequency (F), cross-sectional area (A), Fermi wave vector (k_F), effective mass (m^*), Dingle temperature (T_D), mean free path (l_q), quantum relaxation time (τ_s) and quantum mobility (μ) characterize the dHvA oscillation of $RbTi_3Bi_5$.

	F (T)	A (nm^{-2})	k_F (nm^{-1})	T_D (K)	l_q (nm)	τ_s (s)	μ (m^2·V^{-1}·s^{-1})
$H \parallel c$	190.7	1.816	0.760	7.164	514.024	1.70×10^{-13}	1.026

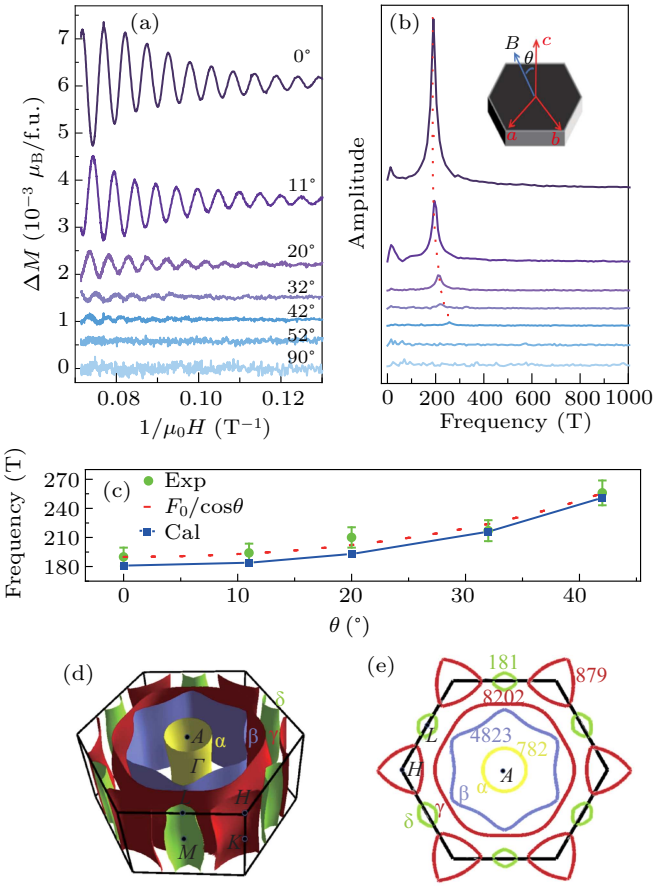


Fig. 3. (a) The dHvA oscillation as a function of $1/(\mu_0 H)$ at various angles. (b) FFT spectra of the dHvA oscillation at different angles. The inset shows the orientation of the magnetic field. The red dotted line is a guide to the eye. (c) Angle dependence of the FFT frequencies. The green point is the experimental results with a 5% error. The red dotted line and the blue solid line represent the $F_0/\cos\theta$ fitting line and the values of theoretical calculations at various angles, respectively. (d) Three-dimensional Fermi surfaces of $RbTi_3Bi_5$. (e) Fermi surface in the $k_z = 0.5$ plane. The black regular hexagon is the first Brillouin zone. The corresponding frequencies are given as numbers in units of Tesla.

Angular dHvA quantum oscillation measurements were performed at 2 K to investigate the detailed Fermi topology shown in Fig. 3(a). To map the fine structure of the Fermi surface, the magnetic field is tilted from the c-axis to the [110] direction by rotating the sample. The angle between the magnetic field and the c-axis is defined as θ. Thus, $\theta = 0°$ denotes the field along the c direction and $\theta = 90°$ denotes the field along the [110] direction. According to the Onsager rule, the Fermi surface area and frequencies of quantum oscillation in magnetic fields can be described as $F = \left(\frac{\hbar}{2\pi e}\right)A$, where A is the Fermi surface area and F is the frequency of the quantum oscillation. The FFT spectra of $\Delta M(H)$ at various angles taken at 2 K are plotted in Fig. 3(b). These oscillations exhibit strong angle dependence and gradually become invisible as the applied field is rotated from the c-axis to the ab plane. The oscillation at $F = 190$ T varnishes for $\theta > 50°$. By using $F_0/\cos\theta$ ($F_0 = 190$ T), the angular-dependent F can be fitted, indicating a typical 2D character for this revealed Fermi surface. To further understand this Fermi topology, DFT calculations were performed to investigate more details of the electronic structure. As shown in Fig. 3(d), multiple Fermi pockets are revealed. Four dispersive bands crossing E_F, labeled α to δ, form one circle-like (α band) and one hexagonal-like (β band) electron pocket. The γ band crosses through E_F twice, forming a hexagonal-like electron pocket around the Brillouin zone (BZ) center and a triangle-like hole pocket around the BZ corner. In addition, the δ band constitutes a rhombic-like hole pocket around the boundary of the BZ. By analyzing these Fermi sheets, the observed oscillation of 190 T is related to the electron δ sheet. This vessel-shaped Fermi sheet located around the M point exhibits a strong 2D character. As shown in Fig. 3(e), the calculated oscillatory frequencies of the δ sheet are consistent with the former experimental results. Correspondingly, the effective mass for the δ bands from the 3d orbit of Ti is calculated to be $0.24m_e$ which is close to the experimental value. The failure to observe quantum oscillations for the other Fermi pockets could be attributed to the large moving orbits of the extremal cross section, which may need further higher-field measurements.

To obtain the exact Berry phase, it is crucial to correctly assign the Landau index to the $\Delta M(H)$ extremum. Based on our experimental results, the minima of ΔM are assigned to be the integer indices and the maxima are assigned to the half-integer indices.[45] The related Landau level fan diagram for the frequency F_β at 2 K is determined and presented in Fig. 4. By fitting the Landau index N as a function of $1/(\mu_0 H)$ at various angles, we obtained Berry phase $\phi_B = 2\pi\left(n_0 - \delta + \frac{1}{2}\right)$. Correspondingly, the angular-dependent Berry phase ϕ_B is around 0 and exhibits angular independence, as shown in the inset in Fig. 4. The DFT calculation reveals three types of nontrivial topological band structures for $RbTi_3Bi_5$. At the K point, the type-II Dirac nodal line is protected by a mirror symmetry without considering the spin–orbit coupling (SOC). A negligible gap opens at the type-II nodal line by including the SOC, which is distinct from the pronounced gaps that Dirac points open at the trivial band-crossing points. This kind of nontrivial topological band structure can usually host additional Berry curvature, resulting in a π shift in Berry phase for quantum oscillations such as that in $CsTi_3Bi_5$. The $\phi_B = 0$ in $RbTi_3Bi_5$ may be attributed to the position of the Dirac nodal line a little further away from the Fermi level. On the other

hand, around the M point, the vHS seems insensitive to additional Berry curvature.

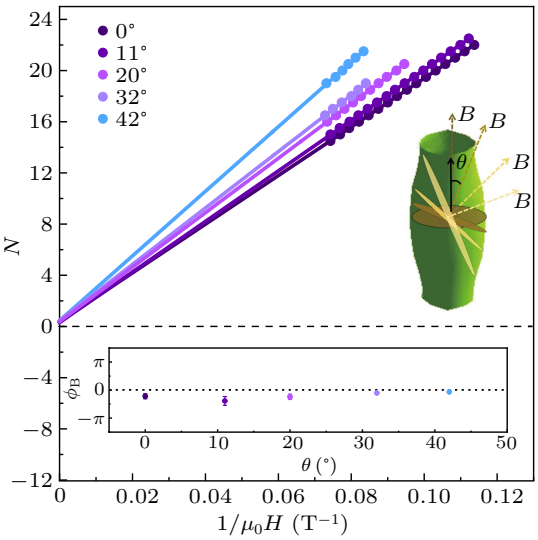


Fig. 4. Landau index N versus $1/(\mu_0 H)$ for the frequency F_β, derived from 2 K at various angles of the magnetic field deviating from the c-axis. The inset shows the Berry phase ϕ_B versus the rotating magnetic field angle θ and the schematic is the Fermi pocket for different magnetic field directions.

Our experimental and theoretical investigations on $RbTi_3Bi_5$ reveal similar electronic structures to those of RbV_3Sb_5. However, the DFT calculations suggest that the vHSs at the M points are a little far away from E_F. The imperfect electronic nesting seems to fail to drive CDW order. Recent research suggested that even if the vHSs are tuned by doping in ATi_3Bi_5 the electronic nesting between the vHSs at the M point alone is insufficient to drive CDW order in these kagome metals.[48] The absence of CDW could be attributed to the different correlation effects or structural instability in various kagome systems.

4. Conclusion

In summary, we have investigated the electronic structure of single crystals of $RbTi_3Bi_5$ by de Haas–van Alphen oscillations. Combined with DFT calculations, four types of Fermi surfaces were revealed. The δ Fermi pocket related to a 190 T quantum oscillation β revealed experimentally exhibits a 2D character. The Landau level fan diagram reveals that the Berry phase of the β oscillation in $RbTi_3Bi_5$ is around zero in contrast to that with a π shift in $CsTi_3Bi_5$. The results suggest that $RbTi_3Bi_5$ is a sensitive candidate material for exploring exotic electronic states and topological correlated physics in kagome systems.

Acknowledgements

Project supported by the National Key Research and Development Program of China (Grant No. 2023YFA1406500), the National Natural Science Foundation of China (Grant Nos. 12174454, U2130101, and 92165204), the Guangdong Basic and Applied Basic Research Funds (Grant Nos. 2024B1515020040 and 2022A1515010035), Guangzhou Basic and Applied Basic Research Funds (Grant No. 2024A04J6417), and Guangdong Provincial Key Laboratory of Magnetoelectric Physics and Devices (Grant No. 2022B1212010008).

References

[1] Yu S L and Li J X 2012 *Phys. Rev. B* **85** 144402
[2] Wang W S, Li Z Z, Xiang Y Y and Wang Q H 2013 *Phys. Rev. B* **87** 115135
[3] Ye L D, Kang M G, Liu J W, von Cube F, Wicker C R, Suzuki T, Jozwiak C, Bostwick A, Rotenberg E, Bell D C, Fu L, Comin R and Checkelsky J G 2018 *Nature* **555** 638
[4] Kong X M, Tao Z C, Zhang R, Xia W, Chen X, Pei C Y, Ying T P, Qi Y P, Guo Y F, Yang X F and Li S Y 2024 *Chin. Phys. Lett.* **41** 047503
[5] Ortiz B R, Gomes L C, Morey J R, Winiarski M, Bordelon M, Mangum J S, Oswald L W H, Rodriguez-Rivera J A, Neilson J R, Wilson S D, Ertekin E, McQueen T M and Toberer E S 2019 *Phys. Rev. Mater.* **3** 094407
[6] Wu X, Schwemmer T, Müller T, Consiglio A, Sangiovanni G, Di Sante D, Iqbal Y, Hanke W, Schnyder A P, Denner M M, Fischer M H, Neupert T and Thomale R 2021 *Phys. Rev. Lett.* **127** 177001
[7] Ortiz B R, Sarte P M, Kenney E M, Graf M J, Teicher S M L, Seshadri R and Wilson S D 2021 *Phys. Rev. Mater.* **5** 034801
[8] Hao Z Y, Cai Y Q, Liu Y X, *et al.* 2022 *Phys. Rev. B* **106** L081101
[9] Shrestha K, Chapai R, Pokharel B K, Miertschin D, Nguyen T, Zhou X, Chung D Y, Kanatzidis M G, Mitchell J F, Welp U, Popović D, Graf D E, Lorenz B and Kwok W K 2022 *Phys. Rev. B* **105** 024508
[10] Li H, Zhao H, Ortiz B R, Park T, Ye M X, Balents L, Wang Z Q, Wilson S D and Zeljkovic I 2022 *Nat. Phys.* **18** 265
[11] Yin Q W, Tu Z J, Gong C S, Fu Y, Yan S H and Lei H C 2021 *Chin. Phys. Lett.* **38** 037403
[12] Zhu H G, Li T R, Yu F H, Li Y L, Wang S, Wu Y B, Liu Z F, Shang Z M, Cui S T, Liu Y, Zhang G B, Zhang L D, Wang Z Y, Wu T, Ying J Y, Chen X H and Sun Z 2023 *Chin. Phys. Lett.* **40** 047301
[13] Li L Y, Yi E K, Wang B, Yu G Q, Shen B, Yan Z B and Wang M 2023 *npj Quantum Mater.* **8** 2
[14] Yang S Y, Wang Y, Ortiz B R, Liu D, Gayles J, Derunova E, Gonzalez-Hernandez R, Šmejkal L, Chen Y, Parkin S S P, Wilson S D, Toberer E S, McQueen T and Ali M N 2020 *Sci. Adv.* **6** eabb6003
[15] Yu F H, Wu T, Wang Z Y, Lei B, Zhuo W Z, Ying J J and Chen X H 2021 *Phys. Rev. B* **104** L041103
[16] Song D W, Zheng L X, Yu F H, Li J, Nie L P, Shan M, Zhao D, Li S J, Kang B L, Wu Z M, Zhou Y B, Sun K L, Liu K, Luo X G, Wang Z Y, Ying J J, Wan X G, Wu T and Chen X H 2022 *Sci. China Phys. Mech.* **65** 247462
[17] Wang Y X, Wu T, Li Z, Jiang K and Hu J P 2023 *Phys. Rev. B* **107** 184106
[18] Mu C, Yin Q W, Tu Z J, Gong C S, Lei H C, Li Z and Luo J L 2021 *Chin. Phys. Lett.* **38** 077402
[19] Mielke C, Das D, Yin J X, *et al.* 2022 *Nature* **602** 245
[20] Luo H L, Gao Q, Liu H X, *et al.* 2022 *Nat. Commun.* **13** 273
[21] Im J H and Kang C J 2023 *Curr. Appl. Phys.* **54** 26
[22] Luo Y, Han Y L, Liu J J, *et al.* 2023 *Nat. Commun.* **14** 3819
[23] Ding G F, Wo H L, Gu Y Q, Gu Y M and Zhao J 2022 *Phys. Rev. B* **106** 235151
[24] Oey Y M, Ortiz B R, Kaboudvand F, Frassineti J, Garcia E, Cong R, Sanna S, Mitrović V F, Seshadri R and Wilson S D 2022 *Phys. Rev. Mater.* **6** L041801
[25] Kato T, Li Y K, Nakayama K, Wang Z W, Souma S, Matsui F, Kitamura M, Horiba K, Kumigashira H, Takahashi T, Yao Y G and Sato T 2022 *Phys. Rev. Lett.* **129** 206402
[26] Zhu C C, Yang X F, Xia W, Yin Q W, Wang L S, Zhao C C, Dai D Z, Tu C P, Song B Q, Tao Z C, Tu Z J, Gong C S, Lei H C, Guo Y F and Li S Y 2022 *Phys. Rev. B* **105** 094507
[27] Zheng L X, Wu Z M, Yang Y, Nie L P, Shan M, Sun K L, Song D W, Yu F H, Li J, Zhao D, Li S J, Kang B L, Zhou Y B, Liu K, Xiang Z J, Ying J N, Wang Z Y, Wu T and Chen X H 2022 *Nature* **611** 682

[28] Du F, Luo S S, Ortiz B R, Chen Y, Duan W Y, Zhang D T, Lu X, Wilson S D, Song Y and Yuan H Q 2021 *Phys. Rev. B* **103** L220504
[29] Yang H T, Ye Y H, Zhao Z, *et al.* 2022 arXiv:2211.12264 [condmat.supr-con]
[30] Werhahn D, Ortiz B R, Hay A K, Wilson S D, Seshadri R and Johrendt D 2022 *De Gruyter.* **77** 757
[31] Jiang Z C, Liu Z T, Ma H Y, Xia W, Liu Z H, Liu J S, Cho S H Y, Yang Y C, Ding J Y, Liu J Y, Huang Z, Qiao Y X, Shen J J, Jing W C, Liu X Q, Liu J P, Guo Y F and Shen D W 2023 *Nat. Commun.* **14** 4892
[32] Li H, Cheng S Y, Ortiz B R, Tan H X, Werhahn D, Zeng K Y, Johrendt D, Yan B H, Wang Z Q, Wilson S D and Zeljkovic I 2023 *Nat. Phys.* **19** 1591
[33] Yang J A, Yi X W, Zhao Z, *et al*. 2023 *Nat. Commun.* **14** 4089
[34] Yi X W, Liao Z W, You J Y, Gu B and Su G 2023 *Research* **6** 0238
[35] Chen X T, Liu X Q, Xia W, Mi X R, Zhong L Y, Yang K Y, Zhang L, Gan Y H, Liu Y, Wang G W, Wang A F, Chai Y S, Shen J Y, Yang X L, Guo Y F and He M Q 2023 *Phys. Rev. B* **107** 174510
[36] Huang J X, Yamakawa Y, Tazai R, Morimoto T and Kontani H 2023 arXiv: 2305.18093 [cond-mat.str-el]
[37] Rehfuss Z, Broyles C, Graf D, Li Y K, Tan H X, Zhao Z, Liu J L, Zhang Y H, Dong X L, Yang H, Gao H J, Yan B H and Ran S 2024 *Phys. Rev. Mater.* **8** 024003
[38] Zhou Y, Chen L, Ji X C, Liu C, Liao K, Guo Z N, Wang J O, Weng H M and Wang G 2023 arXiv: 2301.01633 [cond-mat.supr-con]
[39] Kresse G and Hafner J 1993 *Phys. Rev. B* **47** 558
[40] Blöchl P E 1994 *Phys. Rev. B* **50** 17953
[41] Perdew J P, Burke K and Ernzerhof M 1996 *Phys. Rev. Lett.* **77** 3865
[42] Kokalj A 1999 *J. Mol. Graphics Mod.* **17** 176
[43] Rourke P M C and Julian S R 2012 *Comput. Phys. Commun.* **183** 324
[44] Wang Y, Liu Y X, Hao Z Y, *et al*. 2023 *Chin. Phys. Lett.* **40** 037102
[45] Shoenberg D 1984 *Magnetic oscillations in metals* (New York: Cambridge University press) pp. 290–312
[46] Xia W, Shi X, Wang Y, Ge W, Su H, Wang Q, Wang X, Yu N, Zou Z, Hao Y, Zhao W and Guo Y 2020 *Appl. Phys. Lett.* **116** 142103
[47] Yi X W, Liao Z W, You J Y and Su G 2023 *Research* **6** 0238
[48] Liu B, Kuang M Q, Luo Y, *et al.* 2023 *Phys. Rev. Lett.* **131** 026701